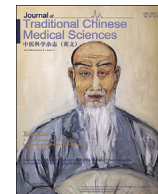




Contents lists available at ScienceDirect

Journal of Traditional Chinese Medical Sciences

journal homepage: www.elsevier.com/locate/jtcms

Essential tremor: A three-dimensional neurosphere *in vitro* model to assess the neurotoxicity of harmane

Rania Aro ^a, Amandine Nachtergaele ^a, Laurence Ris ^b, Mario Manto ^{b,c}, Pierre Duez ^{a,*}

^a Unit of Therapeutic Chemistry and Pharmacognosy, University of Mons(UMONS), Mons 7000, Belgium

^b Department of Neuroscience, Research Institute for Biosciences, University of Mons, Mons 7000, Belgium

^c Department of Neurology, CHU-Charleroi, Charleroi 6000, Belgium

ARTICLE INFO

Article history:

Received 31 August 2022

Received in revised form

5 December 2022

Accepted 5 December 2022

Available online xxx

Keywords:

3D spheroid

Toxicity

Neurotoxicity

Harmane

Essential tremor

ABSTRACT

Objectives: Considering that the 3 Rs of regulation (replacing, reducing, and refining) are meant to reduce the number and suffering of research animals and that current two-dimension (2D) *in vitro* and animals models do not completely mimic the human presentation of the disease, there is a growing demand to develop alternative models. Therefore, we propose here the use of a novel *in vitro* model of three-dimensional (3D) neurosphere cultures to assess neurotoxic or neuroprotective effects with harmane as a model compound.

Methods: A reproducible model of 3D spheroids was developed from embryonic mouse cortical neurons, using molded agarose micro-wells; this method seems particularly practical as it is customizable and widely available and does not require specific cell treatments or assay components different from 2D cultures, allowing for the easy transposition of routine protocols. To assess the neurotoxic effects of harmane, a resazurin assay was performed to measure cell viability, and a highly sensitive fluorometric method, based on the oxidation of dichlorodihydrofluorescein, was applied to measure eventually induced reactive oxygen species (ROS) after exposure to harmane at increasing concentrations of 50 100, and 250 μM .

Results: Hydrogel microwells facilitated the assembly of spheroids containing neurons and glial cells into a complex 3D structure and prevented the agglomeration of spheroids. Exposure to harmane induced cytotoxicity in 3D neural spheroids, which was correlated with harmane concentrations, with a 27% reduction in viability at 250 μM . Harmane that did not induce significant levels of oxidative stress was detected for all tested concentrations.

Conclusion: This 3D neurosphere model mimics a neuronal microenvironment, allowing a fine study of neurodegenerative disorders and the effects of chemicals on the brain. This model opens novel opportunities, not only from a pathogenetic point of view but also from a therapeutic perspective.

© 2022 Beijing University of Chinese Medicine. Production and hosting by Elsevier B.V. This is an open access article under the CC BY-NC-ND license (<http://creativecommons.org/licenses/by-nc-nd/4.0/>).

1. Introduction

The nervous system has many cell types with multiple functions, complex anatomy, and unique structural and functional characteristics. This complex organization makes the evaluation of neurotoxicity and neuroprotection following exposure to chemical, biological, or physical influences a real concern in neurosciences.

Neurotoxicity is conceivable because of direct effects on neural structure, glia–neuron interactions, or the organization and

plasticity of the nervous system. It may target one or more neurons, resulting in the loss of neurons by apoptosis or necrosis, dysfunction of the axons, or disturbance of neurotransmission. Damage could be permanent or reversible, occurring directly after exposure to a toxicant or with a delay, sometimes for years, and it can involve the complete nervous system or a part of it.¹ Neuroprotection preserves the neural structure and function or slows down the progression of neurodegeneration or malfunction by interfering with a cascade of cell death or damage, by helping the nervous system to recover, and/or by providing a protective effect; such neuroprotection can be conceived before or during the progression of nervous system damage.²

* Corresponding author.

E-mail address: pierre.duez@umons.ac.be (P. Duez).

Peer review under responsibility of Beijing University of Chinese Medicine.

<https://doi.org/10.1016/j.jtcms.2022.12.002>

2095-7548/© 2022 Beijing University of Chinese Medicine. Production and hosting by Elsevier B.V. This is an open access article under the CC BY-NC-ND license (<http://creativecommons.org/licenses/by-nc-nd/4.0/>).

The *in vitro* models most widely used in neurotoxicity screening are classical two-dimensional (2D) models based on 2D cell monolayers adherent on flat surfaces. These 2D models primarily consist of cultures of primary cells, cancer cell lines, cells derived from stem cells, and mixed cells; compared with *in vivo* studies, they provide fast, cost-effective, and reliable methods with the ability to control the concentration of a neurotoxicant, the duration of exposure, the cell type, and environment. Moreover, in a suitably installed model, the nutrients, growth factors, and oxygen are equally distributed among the cells. These models offer easy manipulation, high reproducibility, and ability to yield information about the mechanisms of neurotoxicity with fewer ethical issues. Even though 2D cell cultures have proven their capability in cell-based studies, they are unable to faithfully represent a complex *in vivo* environment, which is directly reflected in the results of tests applied to them. Indeed, *in vivo* cells grow within a complex three-dimensional (3D) microenvironment, which limits the relevance of 2D culture systems to an *in vivo* situation and makes them less biologically relevant as they miss complex cell-to-cell interactions.^{3–6} *In vivo* microenvironments and their dynamics are poorly understood and remain a major challenge in developing a representative *in vitro* model. Huang et al. classified the key elements of a cellular microenvironment into the following 4 groups: (1) the neighboring cells, which interact directly through cell-to-cell physical contacts and indirectly via soluble factors and mechanical communication through the fibrous extracellular matrix (ECM); (2) the factors soluble in the aqueous microenvironment, which include basic nutrients and signaling molecules such as hormones and growth factors; (3) the ECM itself, a complex network of noncellular components that provide a biological scaffold and regulate the cell growth, viability, motility, and differentiation; and (4) the physical fields, which include the stress-strain, heat, magnetic, or electrical stimuli that *in vivo* cells respond to.⁷ The adjunct of a third dimension to the culture system allows to introduce these important aspects of ECM, cell-to-cell exchange, spatial organization, nutrient access, cell geometry, and cell mechanics, which affect various receptors engaged in interactions, thereby modulating cell responses and gene/protein expression and closely mimicking the cellular microenvironment.^{8,9} Thus, a 3D model is expected to better mimic the *in vivo* behavior of cells than 2D cultures.^{7,10} This reasoning has led to the development of various models that simulate organs such as retina, intestine, pituitary, heart, brain, or liver.^{11–17} The ability of spheroidal models to predict toxicity has notably been shown, and such cultures are expected to improve toxicology screening tests.^{18–20}

However, the implantation of 3D cultures remains a challenge. On the one hand, many tools have been developed to efficiently produce 3D cultures and can be classified into the following 2 groups: (1) non-scaffold models, which include self-aggregation of spheroids over time in the absence of attachment scaffold at different micro-wells^{21–24} and microfluidic systems²⁵; (2) scaffold models based on solid scaffolds or natural or synthetic hydrogels.^{26–28} On the other hand, the 3D models (1) are grown in limited fluid flows, resulting in nonhomogeneous supply of nutrients and evacuation of metabolic waste, with the formation of necrotic centers; (2) afford limited protection against shear stress related to manipulations; and (3) are prone to agglomeration between spheroids.²⁹ Non-scaffolds seem particularly practical, as they are customizable and widely available and do not require specific cell treatments or assay components different from 2D cultures, which means that routine protocols can be easily transposed.^{30–32}

Essential tremor (ET) is a progressive neurodegenerative and movement disorder that causes involuntary and rhythmic trembling of the hands, head, voice, legs, and trunk, which makes

normal tasks such as eating or writing difficult.³³ The main clinical features of ET consist of kinetic tremor of the arms (tremor occurring during guided voluntary movements) with frequencies of 4–12 Hz, followed by postural and/or kinetic tremor of cranial structures (i.e., neck, jaw, voice).³⁴ Patients usually first become aware of the tremor when holding newspapers or utensils or when reaching for objects. ET is among the most prevalent disabling and poorly understood neurological movement disorders, which especially affects elderly people but also appears in young adults and even during childhood.³⁵ ET is a complex disorder that might be triggered by a combination of intrinsic and extrinsic mechanisms. Regarding the latter, environmental risk factors contribute to the etiology of ET in a considerable proportion of cases. Yet, there has been little discussion in the tremor literature about a clear identification of these factors. Exposure to beta-carbolines, mercury, lead, and organochlorine pesticides has been incriminated.³⁶ Dietary factors have been examined as possible disease contributors (with positive or negative effects) in Parkinson's disease and many other neurological disorders.^{37–39} The dietary epidemiology of ET, however, has not been rigorously studied; therefore, little is known about a possible association between ET and dietary factors. The effects of different lifestyles on ET have been investigated. For example, it has been shown that Mediterranean diet could have a positive effect on reducing the risk of ET, while elevated meat consumption has a negative effect on ET only in men.⁴⁰ Some intrinsic mechanisms, more specifically genetic factors related to familial ET, are recognized, and the susceptible hereditary gene components have been identified.⁴⁰

From the scarce published data, the dietary intake of β -carboline alkaloids (β CAs), including harmane (Fig. 1), has been implicated in the pathogenesis of ET.⁴⁰ Structurally, β CAs are heterocyclic amines, consisting of a combination of five- and six-membered rings, containing 2 amine groups with some structural similarity to 1-methyl-4-phenyl-1,2,3,6-tetrahydropyridine (MPTP) (Fig. 2), which is commonly used to produce major toxin-induced animal models of Parkinson's disease.⁴¹ Like MPTP, β CAs are highly neurotoxic and tremor-producing; they have been linked to ET based on the literature that demonstrated the elevated blood harmane concentration and its presence in post-mortem brain samples of ET patients.^{41,42} Thanks to its lipid solubility, harmane crosses the blood–brain barrier by passive diffusion but also concentrates in the brain through an active uptake mechanism specific for indole compounds.^{42,43} Laboratory animals exposed to harmane and other heterocyclic amines develop an intense and generalized action tremor a few minutes after administration; tremor resembles ET and is accompanied by the destruction of cerebellar

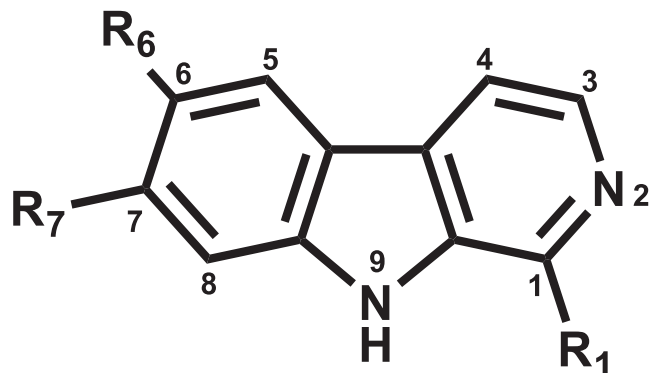


Fig. 1. Chemical structure of β CA ring.

Note: For harmane, $R_1 = \text{CH}_3$, R_6 and $R_7 = \text{H}$.

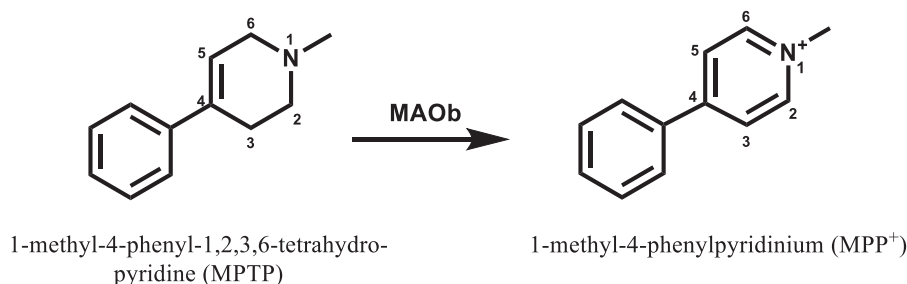


Fig. 2. Chemical structures of the neurotoxin 1-methyl-4-phenyl-1,2,3,6-tetrahydropyridine (MPTP) and its bioactivation by MAOB to its toxic metabolite 1-methyl-4-phenylpyridinium (MPP⁺).

tissues.^{44–46} Humans are exposed to these alkaloids daily through the diet and other environmental factors. β CAs are natural indole alkaloids and are widely distributed in nature β CAs, including various plants and foodstuffs. These compounds have been first detected in *Peganum harmala* L. (*P. harmala*, Luo Tuo Peng), a plant known for inducing hallucinations and used in traditional medicine for its antimicrobial, analgesic, antinociceptive, and abortion effects^{47–49}, but are also present in many other plants such as *Banisteriopsis caapi* (used to prepare the psychoactive beverage ayahuasca), *Tribulus terrestris* L. (*T. terrestris*, Ci Ji Li, an important traditional Chinese medicine widely used as a diuretic and cough expectorant and for the treatment of skin pruritus, red eye, headache, and vertigo),^{50,51} and in *Nicotiana tabacum* leaves and cigarette smoke.⁵² In addition, these compounds are endogenously generated in human tissues and the brain.^{53,54} Of note, the neurotoxicity of β CAs depends on the dose; namely, high or chronic doses trigger neurotoxicity,⁵⁵ while low doses may increase dopamine levels and perhaps even present protective properties.⁵⁶ To achieve neuroprotection, both monoamine oxidase A (MAOA) and monoamine oxidase B (MAOB)—the enzymes responsible for catalyzing oxidation of biogenic amines—should be inhibited to a certain extent. This inhibition decreases the production of detrimental reactive oxygen species (ROS), a primary factor in neurodegeneration. Interestingly, β CAs (norharmane and harmane), which have been identified in cigarette smoke, can inhibit MAO enzymes.⁵⁷ This inhibition may explain the reduced risk of Parkinson's disease in smokers.⁵⁸ Nevertheless, it should be emphasized that although neurodegenerative diseases share many pathological features such as oxidative stress, iron accumulation, excitotoxicity, and elevated ROS production,⁵⁹ the neuroprotective action of tobacco smoke cannot be generalized to other neurodegenerative diseases, such as Alzheimer's disease.⁶⁰

The lack of clear mechanisms for ET development impedes biochemistry-based studies; in addition, animal models do not reproduce human tremor perfectly, remain expensive, and raise ethical issues. The 3D cell cultures and organoids are being growingly used to bridge the gap between *in vitro* 2D cell cultures and *in vivo* animal models. There is a consensus that 3D models are more physiologically relevant than biochemical assays and 2D cell cultures, as they more closely represent the microenvironments, cell-to-cell interactions, and biological processes that occur *in vivo*.^{61–63} Moreover, 3D neural spheroids are promising in the research of neurological diseases as they may allow to carry out screening studies to identify toxicological effects of environmental factors, including harmane. However, 3D neuronal cultures remain challenging for many technical reasons.

In this study, we aimed at investigating the effect of harmane *in vitro* on an original 3D neurosphere model adapted from Dingle et al.⁶⁴ This model was based on a non-scaffold technique, which requires reasonable lab equipment and offers reproducible

cultures, using prenatal mice neural cells and agarose-molded wells. We developed our model by testing different microwell diameters and cell densities. The ease of harvesting and the reproducibility of neurosphere with 400 μ m diameter produced with large molds made it our choice for the assessment of harmane neurotoxicity. This 3D embryonic neural culture contained neurons and glia; as a single embryo yields a large number of 3D organoids (typically, more than 400), this attractive model can be used to study the pathogenesis of central nervous system (CNS) diseases and the neurotoxicity of compounds and to develop novel therapeutic strategies.

2. Materials and methods

2.1. Ethical approval

All animal procedures and experiments were performed in accordance with the guidelines established by the European Communities Council (Directive 2010/63/EU of March 4, 2014) and were approved by UMONS veterinary ethics committee of the Faculty of Medicine and Pharmacy (LA150002).

2.2. Materials

2.2.1. Preparation of 3D micro Petri Dishes

MicroTissues® 3D Petri Dish® 24-96 and 24-35 were obtained from Merck (Darmstadt, Germany) and UltraPure™ Agarose (Invitrogen) from Fisher (Merelbeke, Belgium).

2.2.2. Cell culture

Cell strainer with 40 μ m pore size was purchased from Merck (Darmstadt, Germany). Hank's Balance Salt Solution (HBSS) (Gibco), Neurobasal® Electro Medium (Gibco), B-27® Electrophysiology (Gibco), Glutamax® (Gibco), fetal bovine serum (FBS, Gibco; EU-approved; heat-inactivated for 30 min at 56 °C), and penicillin-streptomycin (Gibco) were obtained from Fisher (Merelbeke, Belgium).

2.2.3. Immunocytochemistry

Casein of high-purity grade and glass-bottom confocal slides were obtained from VWR (Leuven, Belgium). In addition, 12-well removable chambers, polyethylene glycol from Ibidi (Gräfelfing, Germany), MAP2 antibody (rabbit), GFAP antibody (rabbit), GFAP antibody (mouse), goat anti-rabbit IgG (H + L) cross-adsorbed secondary antibody Alexa Fluor 594, goat anti-rat IgG (H + L) cross-adsorbed secondary antibody Alexa Fluor 594, goat anti-rabbit IgG (H + L) cross-adsorbed secondary antibody Alexa Fluor 488, and goat anti-rat IgG (H + L) cross-adsorbed secondary antibody Alexa Fluor 488 were purchased from Thermo Fisher (Waltham, MA). Anti-Tau antibody was purchased from Abcam

(Cambridge, United Kingdom), and Anti-Iba-1 was obtained from Wako Chemicals (Neuss, Deutschland). Anti- β -tubulin, polyethylene glycol (PEG) 8000, formamide of biology grade, and 4', 6-diamidino-2-phenylindole (DAPI) were purchased from Merck (Darmstadt, Germany).

2.2.4. Cytotoxicity and ROS

Harmane (98%) was obtained from Merck (Darmstadt, Germany); CellEvent caspase 3/7 green (Invitrogen), staurosporine, and propidium iodide 1.0 mg were obtained from Thermo Fisher (Waltham, MA); resazurin sodium salt dichlorodihydrofluorescein diacetate was obtained from Merck (Darmstadt, Germany).

2.2.5. Microscopy

The images were acquired using a laser scanning confocal microscope (LSM 710) equipped with an Airyscan detector, spectral (32-channels) PMT detector, and 7 laser lines, driven by the ZEN blue software (Zeiss, Oberkochen, Germany); Olympus IX 70 inverted fluorescence phase contrast microscope, equipped with a Hamamatsu digital camera C11440, LED illuminator pE-340 fura, and 2 filter cube U-MWIG3 and U-MWIBA3, driven by the Cell dimension software (Olympus, Tokyo, Japan); and field-emission scanning electron microscope (JSM-7200F), operating at 2 kV with secondary electron detection, after metallization with a JFC 1100E ion-sputtering device (JEOL, Tokyo, Japan).

2.3. Methodology

2.3.1. Preparation of 3D micro Petri Dishes

To obtain agarose hydrogel micro-wells with round-bottomed recesses, 330 μ L of 2% molten agarose in sterile saline (0.9% w/v NaCl) was pipetted in 24-well plates 3D Petri Dish® (#24–35 large, MicroTissues®), with each micro-mold forming 35 micro-wells or 96 micro-wells. Upon solidification, agarose was carefully removed, transferred to a standard 24-well tissue culture dish, equilibrated with complete cell culture medium (Neurobasal® Electro Medium supplemented with 2% B-27® electrophysiology, 0.25% Glutamax®, 1% FBS, 0.5% streptomycin-penicillin), and then incubated in a 5% CO₂ humidified incubator at 37 °C. Since the agarose hydrogel was transparent, the spheroids could be easily viewed using a standard inverted microscope.

2.3.2. Cell isolation

Primary cultures of dissociated hippocampal and cortical neurons were isolated from mouse BL6 E17 embryos. After mouse dissection, the brains of the embryos were placed in cold HBSS; hemispheres were divided; the brainstem and cerebellar tissues were discarded; and the meninges were removed. The hippocampus and cerebral cortex were collected and transferred to a 15-mL conical tube containing HBSS and gently triturated by pipetting with P1000 pipette until visual homogeneity. The suspension was filtered with a cell strainer (40 μ m pore size); then 10 mL of Neurobasal® medium with 10% FBS was gently added, and the cell suspension was centrifuged (312 \times g, 10 min, 4 °C). The supernatant was discarded, and the cells were resuspended in a complete Neurobasal medium at room temperature (RT); the cells viability and counting were determined using trypan blue.

2.3.3. 3D neural spheroid production

The medium equilibrating the agarose microwells was removed; the cell suspension was diluted with warmed complete Neurobasal medium (at 37 °C) to the desired seeding density based on MicroTissues® protocol (Tables 1 and 2).⁶⁵ For the continuation of the work, the diameter-selection criteria depended on the reproducibility and handling easiness. The cells were seeded onto the

Table 1

The large 3D micro-dishes (24–35) with the cell seeding numbers for different spheroid diameters.

Nominal spheroid diameter	Cells/spheroid	Total cells seeded (cells/75 μ L)
200	1000	35 000
400	8000	280 000
500	15 625	547 000
700	42 875	1 500 000

Note: 24-well plate; smaller spheroids: 35.

Table 2

The small 3D micro-dishes (24–96) with the cell seeding numbers for different spheroid diameters.

Nominal spheroid diameter	Cells/spheroid	Total cells seeded (cells/75 μ L)
50	15	35 000
100	125	12 000
200	1000	96 000
300	3375	324 000

Note: 24-well plate; smaller spheroids: 96.

agarose gels and incubated in a 5% CO₂ humidified incubator at 37 °C. After 30 min, 1 mL of complete Neurobasal medium was added slowly (on the board of the plate); 24 h after seeding, the medium was removed fully and replaced with fresh complete Neurobasal; then, cells/spheroids were fed every 3–4 days by removing half of the old medium and replacing it with the same volume of a fresh complete Neurobasal medium.

2.3.4. Immunocytochemistry

The protocols of immunostaining and clearing protocols were inspired from Dingle et al.⁶⁴ and from protocols of the University of Mons (UMONS) Neuroscience Department. After 2 weeks of neuron culturing, the spheroids were washed 3 times with warmed (37 °C) phosphate-buffered saline (PBS, pH 7.4), fixed overnight at RT with 4% paraformaldehyde (PAF) in PBS at pH 7.4, washed with PBS, and stored in 0.07% sodium azide PBS. To permeabilize the spheroids and improve the penetration of antibodies, the spheroids were incubated in a solution of PBS containing 0.2% Triton X-100 (1 h, twice), followed by incubation in a blocking solution of casein 0.5% and NH₄Cl 5% in PBS (2 h, RT). The spheroids were transferred to glass-bottom confocal slides or 12-well removable chamber slides using a P-1000 pipette with end-cut tips (to minimize the damage to spheroids), incubated (48 h, RT) in primary antibodies diluted with the blocking solution, washed with PBS/Triton X-100 0.2% (1 h, twice), and incubated (48 h, RT) in secondary antibodies diluted with the blocking solution (Table 3). To stain the DNA, the spheroids were then washed with PBS/Triton X-100 0.2% (1 h, RT, twice), counterstained with DAPI 0.5 μ g/mL in PBS/Triton X-100 0.2% (1 h, RT), and then rinsed with PBS.

Table 3

Primary and secondary antibodies for immunohistochemistry.

Antibodies	Host	Reactivity	Class	Dilution
<i>Primary</i>				
MAP2	Rabbit	Human, mouse, rat	Polyclonal	1:200
Anti-Tau	Mouse	Human, mouse, rat	Monoclonal	1:100
GFAP	Mouse	Human, mouse	Monoclonal	1:200
GFAP	Rabbit	Human, mouse, rat	Polyclonal	1:250
Iba-1	Rabbit	Human, mouse, rat	Polyclonal	1:200
Anti- β -tubulin	Mouse	Human, bovine, rat	Monoclonal	1:100
<i>Secondary</i>				
Alexa Fluor 594	Goat	Mouse	Polyclonal	1:200
Alexa Fluor 488	Goat	Rabbit	Polyclonal	1:200
Alexa Fluor 594	Goat	Rabbit	Polyclonal	1:200
Alexa Fluor 488	Goat	Mouse	Polyclonal	1:200

For Clear^{T2} clearing, the 3D spheroids were incubated with 25% formamide/10% PEG in PBS for 10 min, then in 50% formamide/20% PEG in PBS for 5 min, followed by 50% formamide/20% PEG in PBS for 60 min as the final mounting solution.

2.3.5. Cytotoxicity

Given the difficulty to perform a microscopic measurement of the spheroids, the method proposed by Pamies et al.,⁶⁶ based on measuring fluorescence in the culture media, was selected. On day 14 of culture, the medium was fully replaced with a fresh medium containing the tested harmaline concentrations of 50, 100, and 250 μM prepared from a stock solution of harmaline 10 mM in PBS and 10% dimethyl sulfoxide (DMSO); maximal DMSO concentration in contact with the spheroids, 0.25%. To measure the cell viability, a resazurin assay was performed.⁶⁶ Resazurin (7-hydroxy-3H-phenoxazin-3-one 10-oxide) is a blue dye, which is used as a redox indicator for aerobic and anaerobic respiration. It is irreversibly reduced to fluorescent resorufin.⁶⁷ After 21 h of exposure to the different harmaline concentrations, resazurin (50 μL of a 2 mg/mL stock solution in PBS) was directly added to the medium of 24-well plates (1 mL/well). After incubation for 3 h at 37 °C and 5% CO₂, 50 μL of the medium of each well was transferred to a 96-well plate, and the fluorescence intensities were measured at 525 nm/580–640 nm (excitation/emission) with a multi-well fluorometric reader GloMax®-Multi + Microplate Multimode reader (Promega, Madison, WI). These viability results were compared with the fluorescence intensity measurements corresponding to cells, neurons, and glial cell after 24 h of exposure to the different concentrations of test compounds. The images were acquired using an Olympus IX 70 fluorescence microscope, equipped with a Hamamatsu digital camera C11440, LED illuminator pE-340 fura, and 2 filter cube U-MWIG3 and U-MWIBA3, driven by the Cell dimension software. The fluorescence intensities were measured by Fiji software (open source).

2.3.6. ROS measurement

A highly sensitive fluorometric method was used to measure ROS.⁶⁸ This method was based on the oxidation of 2',7'-dichlorodihydrofluorescein (DCFH) to the fluorescent 2',7'-dichloro-fluorescein (DCF) by the free radicals generated in the medium. DCFH was prepared by hydrolysis of 2DCFH di-chlorodihydrofluorescein diacetate (DCFH-DA) as described by Cathcart and coworkers.⁶⁹

After 3, 5, 9, and 24 h of harmaline exposure, 50 μL of the medium was collected, transferred to a 96-well-plate, and incubated with 50 μL of DCFH for 45 min at 37 °C and 5% CO₂. The fluorescence intensity was measured at 490 nm/510–570 nm (excitation/emission) in a multi-well fluorometric reader GloMax®-Multi + Microplate Multimode reader (Promega, Madison, WI).

2.3.7. Study of apoptotic and necrotic effects

On the 14th day of culture, we collected the neurospheres using a pipette and transferred them to slides with a removable 12-well silicone chamber (Ibidi®, Gräfelfing, Germany). We replaced the entire medium with a fresh medium with different harmaline concentrations. Staurosporine at a concentration of 200 nM was a positive control for apoptosis, while hydrogen peroxide at a concentration of 50 μM was a positive control for oxidative stress, which mainly results in necrosis.

2.3.8. Statistical procedures

The SigmaPlot 11 software (Systat Software, San Jose, CA) was used for statistical analysis. One-way, two-way, and three-way ANOVA tests were performed, with a Shapiro–Wilk test for normality, a Brown–Forsythe test for equal variances, and a post-hoc Bonferroni test for post-hoc pairwise multiple comparisons.

All data are shown as means \pm standard deviation (SD) of at least three biologically independent experiments performed with three technical replicates. Statistical significance was set at $P < .05$.

3. Results

3.1. The assembly of neural cells into 3D spheroids

To define optimal conditions, monodispersed cortical cells obtained from the mice embryos were seeded in the micro-molded agarose wells at different seeding densities in the small (8 \times 12 array) and large (7 \times 5 array) mold-casted gels. The hydrogel microwells facilitated the assembling of the cells while preventing the agglomeration between spheroids; the aggregation of the cells in the spheroids was noticed on day 4. After several cell cultures with different spheroid diameters (Figs. 3 and 4), we determined that (1) the spheroids with the diameter of 50 and 100 μm in the small molds and 200 μm in the large mold were not reproducible; (2) the spheroids with the diameter of 300 μm in the small mold and 500 and 700 μm in the large mold were difficult to harvest; and (3) the spheroids with 200 μm in the small molds and 400 μm in the large molds were the best, both in terms of size reproducibility and harvest easiness. We assumed that the biggest spheroids would be more representative of the real cell environment; thus, the spheroids with 400 μm in diameter obtained at a seeding density of 8000 cells/micro-well from large (7 \times 5 array) mold-casted gels were our choice for the continuation of the work.

Although this method requires simple laboratory equipment, it needs a very careful and precise experimenter as different factors affect the quality and quantity of spheroids, starting from the setup prior to culture and ending by spheroid harvest: (1) the quality of agarose micro-well shapes affects the distribution of cells and thus the diameter of spheroids; (2) the pre-culture equilibration with the medium; (3) the dissection and dissociation of cortical tissues influence the quality of neurons seeded; (4) the time needed for cells to settle and aggregate before adding the total volume of medium; and (5) the regular and timely medium renewal.

3.2. Spheroid's diameter

Monodispersed cortical cells were seeded in the large micro-molded hydrogels at seeding densities of 8000 cells per micro-well. The spheroid diameters on the first day *in vitro* (1 DIV) ranged from 500 to 700 μm , and we noticed their aggregation from 4 DIV. The spheroid diameter increased from 8 to 11 DIV; between 11 and 14 DIV, a reduced diameter growth was observed. The diameter measurement of three biologically independent experiments performed with 3 technical replicates indicated a mean diameter of $626 \pm 81 \mu\text{m}$ on the first day, $363 \pm 39 \mu\text{m}$ on day 4, $356 \pm 39 \mu\text{m}$ on day 8, $392 \pm 31 \mu\text{m}$ on day 11, and $394 \pm 37 \mu\text{m}$ on day 14. A two-way ANOVA for the diameter with factors “time” and “culture” indicated that the differences in the mean values among the different days were greater than that would be expected by chance ($P \leq .001$) (Fig. 5).

The measurements of spheroid diameters indicated that the spheroids were well aggregated at 4 DIV, with a growth observed between 8 and 11 DIV. Depending on the growth time, the measured diameters were slightly different from culture to culture, but became uniform on 11 DIV.

Based on our experience, different parameters can be improved to yield a reproducible diameter culture: (1) making sure that the agarose mold does not form a curved contact surface with the plate; (2) automatizing cell counting; and (3) suspending the cells very well before seeding.

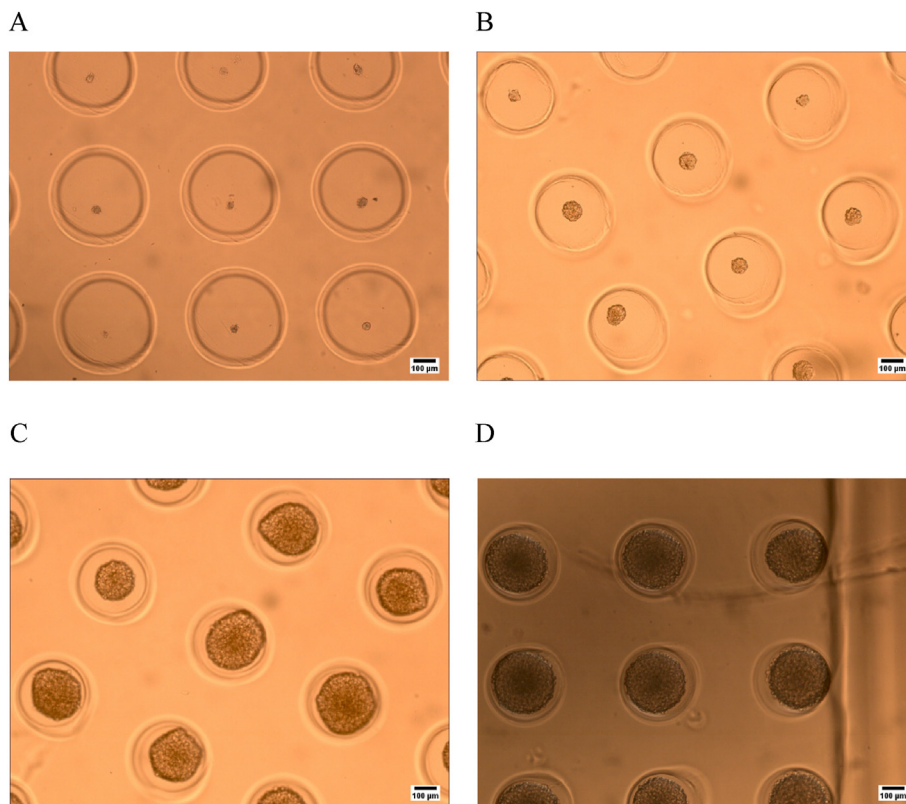


Fig. 3. Visible light contrast microscopy images of neurospheres in small micro-wells on day 14, with seeding of monodispersed mice embryos cortical cells at initial densities of (A) 15 cells/spheroid and 50 μm in diameter, (B) 125 cells/spheroid and 100 μm in diameter, (C) 1000 cells/spheroid and 200 μm in diameter, and (D) 3375 cells/spheroid and 300 μm in diameter.

Note: Magnification: $5\times$. Scale bar = 100 μm .

3.3. Spheroid structure

3.3.1. Spheroid surface structure

The appearance of spheroids was analyzed by scanning electron microscopy (SEM). On SEM images, the spheroids had a characteristic 3D appearance, and these images were useful for evaluating the surface structure of the spheroids. Based on that, we observed the following 2 types of morphologies (Fig. 6): (1) spheroids with hypercellularized surface, and (2) spheroids with more regular shape and structure, with dispersed cells. The characterization of the surface structure by SEM reflected the intricacy of cell-to-cell connections, with complex surfaces and a bundle of axons and dendrites (Fig. 7).

3.3.2. Identification and quantification of cell types

3.3.2.1. By fluorescence microscopy. CNS marker, based immunocytochemistry coupled with fluorescence microscopy, allowed us to identify neuronal cells by tracing dendrites through microtubule-associated protein 2 (MAP2) expression, astrocytes through glial fibrillary acidic protein (GFAP) expression, and nuclei through DAPI staining (Fig. 8). Normalizing the fluorescence intensity based on cell numbers is unrealistic in 3D. Thus, even though it is not ideal, we selected to normalize the fluorescence based on the spheroid diameter by hypothesizing that spheroids with close diameters have similar radii and close cell numbers.

To determine the variability of the proportion of cell types in the neurosphere among the different cultures, the intensities of fluorescence were measured for the different biomarkers and compared in 3 biologically independent experiments with 3 technical replicates. One-way ANOVA indicated that the *P*-value for the difference between the groups was higher than 0.05, which

indicates that the proportions of neurons, nuclei, and glial cells in our neurospheres did not differ from culture to culture (Fig. 9).

3.3.2.2. By confocal microscopy. The confocal microscopy images showed that neurons and glial cells formed complex 3D structures in the spheroids. The neurons were stained by anti-neuronal antibodies, including MAP2, beta III tubulin, and Tau; among the glial cells, astrocytes were marked by GFAP and microglia were marked by ionized calcium-binding adapter molecule 1 (IBA-1). The confocal images (Figs. 10 and 11) yielded higher sensitivity than fluorescence images, better signal-to-noise ratios, and higher X, Y, and Z resolution while maintaining high-throughput data. However, the imaging penetration depth, increased light absorption, and light scattering did not allow us to gather information from more than 100 μm of depth. A water immersion objective with $40\times$ magnification was supposed to enable higher resolution and details at greater depth; however, its use was more challenging as the average diameters of 400 μm spheroids were too big for $40\times$ magnification. For smaller spheroids, we were able to obtain a better resolution, but the depth could not surpass 100 μm , even when applying clearing techniques. Therefore, the confocal images were used for identification only, as it was challenging to obtain high-quality images from the depth with our thick 3D neuronal spheroids.

3.3.2.3. By sectioning/staining. The dark centers observed in the spheroids on confocal imaging raised the question as to whether these are due to a light penetration issue or due to the occurrence of necrotic centers and/or central acellular matrices. To clarify this issue, automated slice sectioning followed by hematoxylin and eosin (H&E) staining and examination under visible light was

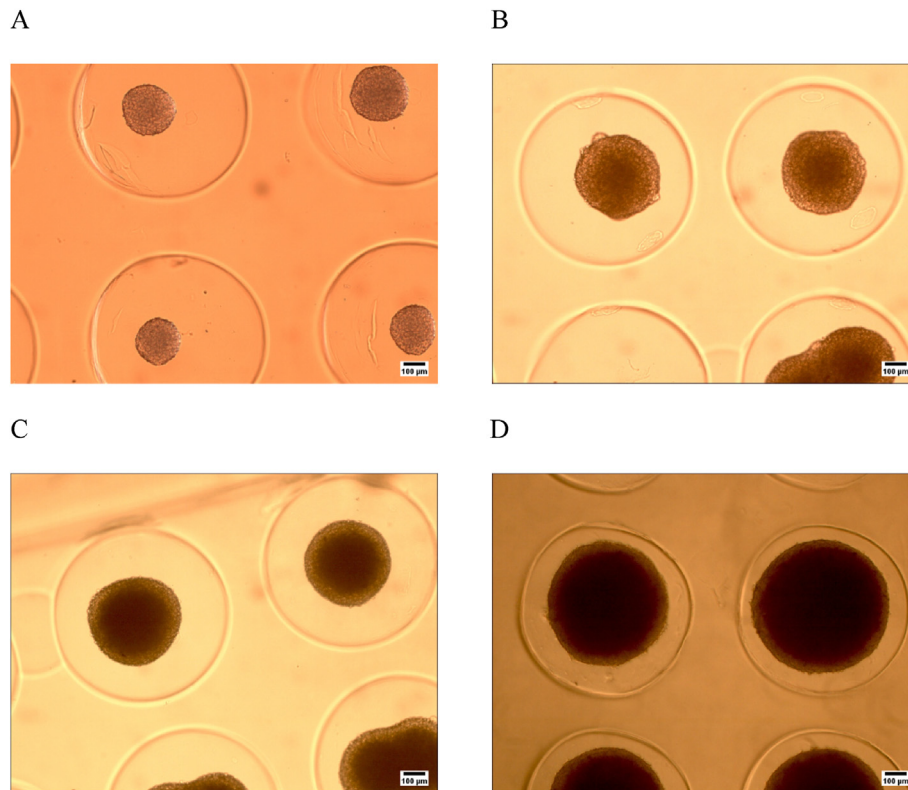


Fig. 4. Visible light contrast microscopy images of neurospheres in large micro-wells on day 14, with seeding of monodispersed mice embryo cortical cells at initial densities of (A) 1000 cells/spheroid and 200 μm in diameter, (B) 8000 cells/spheroid and 400 μm in diameter, (C) 15,625 cells/spheroid and 500 μm in diameter, and (D) 42,875 cells/spheroid and 700 μm in diameter.

Notes: Magnification: $5 \times$. Scale bar = 100 μm .

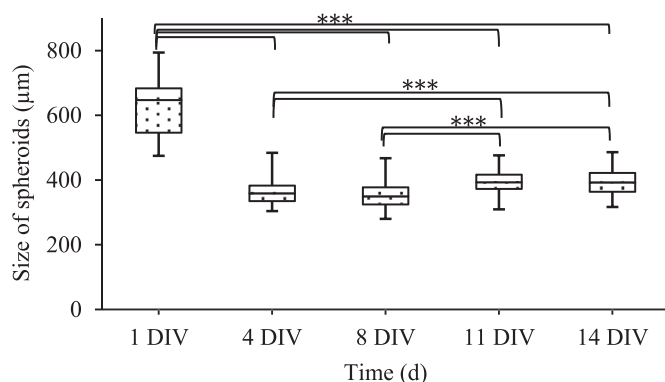


Fig. 5. Spheroid diameters (8000 monodispersed mice embryos' cortical cells/spheroid) from 1 to 14 DIV from 3 independent experiments with 3 technical replicates.

Note: The diameter decreased with the aggregation between 1 and 4 DIV ($P < .001$); the mean diameters were stable between 4 and 8 DIV ($P = 1$); and then they increased till 11 DIV ($P < .001$) and were stable to 14 DIV ($P = 1$). $n = 54$.

applied to the neuronal spheroids. The obtained images indicated that there was no necrosis in the center but fewer cells that seemed embedded in a loose connective tissue (Fig. 12).

3.4. Harmane and 3D neural spheroid viability

After exposure to the increasing concentrations of harmane (50, 100, 250 μM) for 24 h, the 3D neural spheroids showed a decrease in cell viability (resazurin test), which correlated with harmane concentration, down to 27% reduction at 250 μM harmane. As the

data were normally distributed (Shapiro–Wilk test, $P = .848$), these were compared by a two-way ANOVA test, with the factors “harmane concentration” and “experiment.” The difference was statistically significant for the factor “harmane concentration” ($P < .001$) and not statistically significant for factors “experiment” and “harmane concentration \times experiment” ($P = .402$ and $.121$, respectively). Post-hoc pairwise t tests (Bonferroni correction) indicated that the differences were statistically significant for both 250 and 100 μM vs. the control group, with $P < .001$ and $P = .006$, respectively (Fig. 13).

For verification of these resazurin viability data, we measured the intensity of fluorescence of neurons (MAP2), glial cells (GFAP), and nuclei (DAPI) after 24 h exposure to the different concentrations of harmane. We noticed a reduction in the intensity of fluorescence for the 3 stains, which corresponded to the increase in harmane concentrations (Fig. 14). A two-way ANOVA was applied with the “harmane concentration” and “experiment” factors, and we found a statistically significant effect of “harmane concentration” ($P < .001$ for nuclei, neurons, and glial cells). The effects of “experiment” were not statistically significant for nuclei and glial cells ($P = .524$ and $.375$, respectively), but were statistically significant for the fluorophore of neurons ($P = .014$). The “harmane concentration \times experiment” factor was statistically significant for neurons ($P < .001$) and not significant for nuclei and glial cells ($P = .2$ and $.4$, respectively).

Despite the huge variability inherent to this experiment (variability that inevitably arises from the different variabilities we have investigated, i.e., the sizes of spheroids and the distribution of the different types of cells), the absolute fluorescence intensities indicate a clear but nonsignificant trend in reduction of viability with harmane concentration (Fig. 14A). When expressed in percentages of control

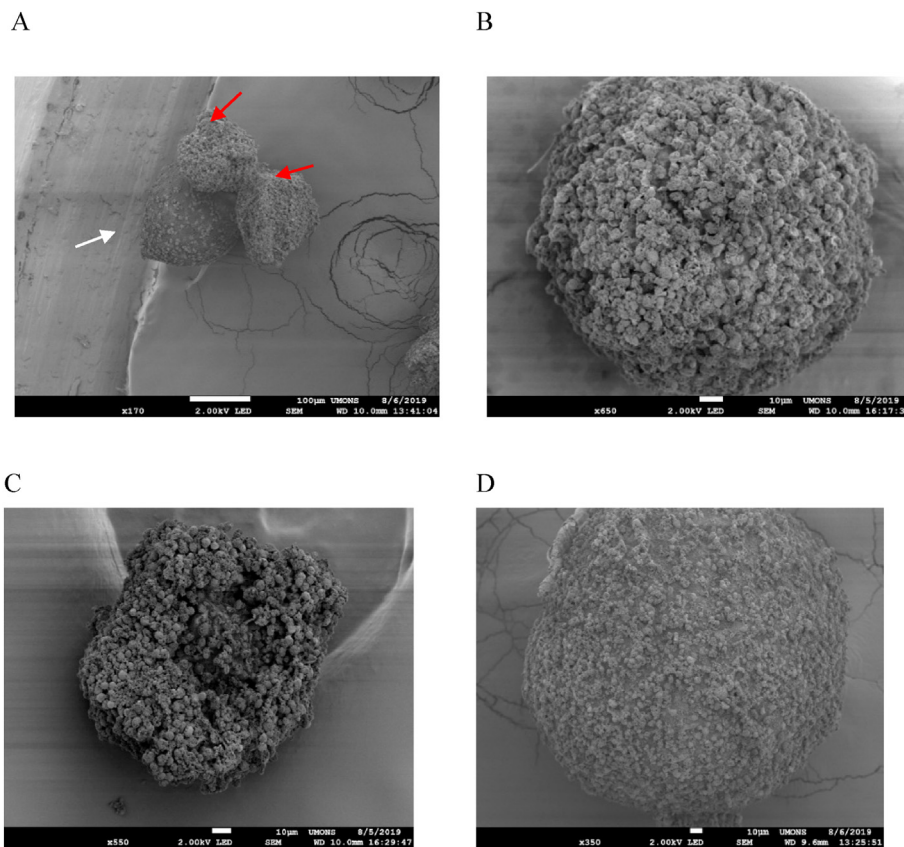


Fig. 6. SEM images of the 2 types of spheroids observed, a spheroid with a hypercellularized surface (A, red arrows; and B, C), and spheroids with a more regular, well-shaped surface (A, white arrow; D).

Notes: The cells of the hypercellularized spheroids present irregular membranes probably damaged by the fixing solution (PAF 4%) or in dehydration or drying steps. The presence of smooth then porous sections and incomplete spheres supports this hypothesis. However, the spheroids with the highest diameter might not be fully dehydrated, which explains their more regular shape. Magnification: 170 × in A, 650 × in B, 550 × in C, 350 × in D. Scale bar = 100 μm in A, and scale bar = 10 μm in B, C, and D.

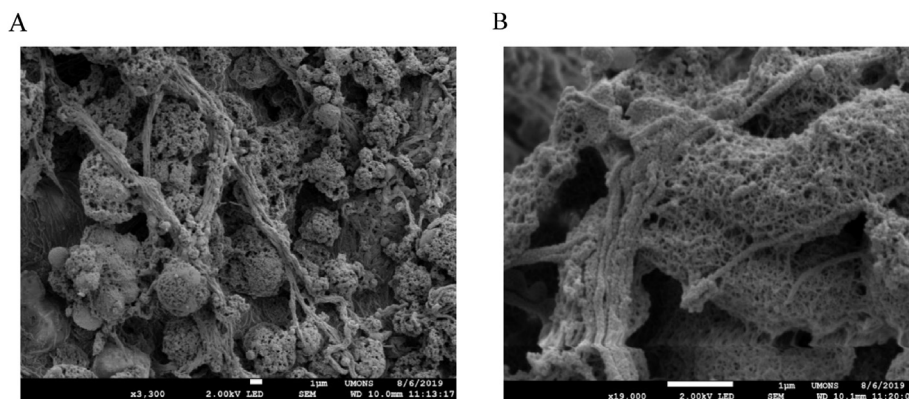


Fig. 7. Bundles of cellular extensions grouped into complex structured (A) and oriented networks (B) on the hypercellularized surface of a spheroid.

Notes: Magnification: 3300 × in A, 19000 × in B. Scale bar = 1 μm.

fluorescence, the trends appear clearer and the cytotoxic effect of harmaline is significant for total cells (nuclei) at 100 and 250 μM (Fig. 14B) and for neurons and glial cells at 250 μM (Fig. 14C and D).

3.5. ROS measurement

After 3, 5, 9, and 24 h of exposure of spheroids to the increasing concentrations of harmaline (50, 100, 250 μM), the medium was collected and mixed with DCFH; after 45 min, the fluorescence of oxidized DCF was measured. The fluorescence intensities were normalized by dividing the measured intensities into the average

measured intensity of negative control. There was a minute variation in ROS production according to harmaline concentration treatments and time, but there were no statistically significant difference for factors “time,” “treatment,” and “experiment,” (three-way ANOVA, $P = .055$ for the factor “time,” $P = .721$ for the factor “treatment,” $P = .1$ for the factor “experiment”) (Fig. 15).

3.6. Study of apoptosis and necrosis on spheroids

Among the 2420 neurospheres produced, after harvesting, 39 were excluded from the experiment because of induced damage

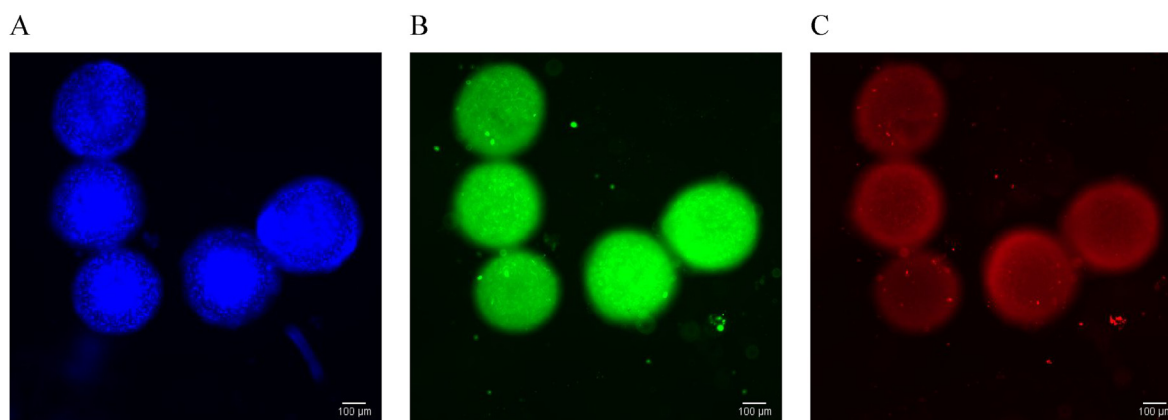


Fig. 8. Fluorescence microscopy images of neuronal spheroids after immunostaining with mouse GFAP monoclonal antibodies (astrocytes), rabbit MAP2 polyclonal antibodies (neurons), goat anti-mouse IgG Alexa Fluor 488, and goat anti-rabbit IgG 594, followed by nuclear staining by DAPI, (A) the nuclei with DAPI; (B) the glial cells with GFAP; and (C) the neurons with MAP2.

Notes: Magnification: $10 \times$. Scale bar = 100 μm .

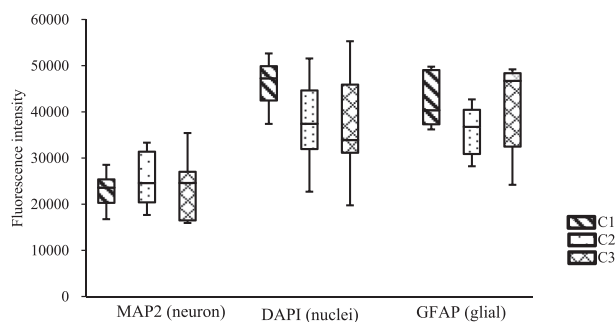


Fig. 9. Comparison of three cultures: fluorescence intensity of neuronal cells and nuclei.

Notes: Mean values of MAP2, DAPI, and GFAP fluorescence intensities, which represent neurons, nuclei, and glial cells, respectively, in three biologically independent experiments performed with three technical replicates. MAP2: microtubule-associated protein 2; GFAP: glial fibrillary acidic protein; DAPI: 4',6-diamidino-2-phenylindole. Bar in the box represents the median of data. There was no statistically significant difference between the experiments ($P > .05$), $n = 9$.

while pipetting to transfer the spheroid (bubble in the medium or damaged surface), and 63 were excluded as they were smaller than 340 μm or larger than 460 μm ; this size range ($400 \mu\text{m} \pm 15\%$) was arbitrarily selected to reduce the interference of diameters on measurements, and the percentage of the excluded spheroids was 4.17%. Alterations in cell morphology occur in both necrotic and apoptotic cells and can be determined by the assessment of staining using fluorescent stains and fluorescence microscopy (Fig. 16).

3.6.1. Measurement of apoptosis

For apoptosis, we measured the fluorescence intensity induced by the activation of the caspase cascade in neurospheres after 24 h exposure to different concentrations of harmame (0–250 μM), staurosporine 200 nM (apoptosis-positive control), or 50 μM H_2O_2 (necrosis-positive control) (Fig. 16). The fluorescence intensity increased with the increased concentration of harmame. A two-way ANOVA was applied for the factors “treatment” and “culture” and for the interaction “treatment” \times “culture,” indicating that the differences were statistically significant for all factors ($P < .001$) (Fig. 17). Post-hoc Bonferroni t tests showed a statistically significant difference between the negative control group and harmame 250 μM and staurosporine 200 nM ($P < .001$).

3.6.2. Measurement of necrosis

To assess necrosis, we measured the fluorescence intensity of propidium iodide in the same conditions as for caspases. We observed an increase in the propidium iodide fluorescence in spheroids exposed to different treatments compared with the control group (Fig. 18). A two-way ANOVA for the factors “treatment” and “culture” and for the interaction “treatment” \times “culture” indicated that the differences were statistically significant for the 3 factors ($P < .001$). Post-hoc Bonferroni t tests showed a statistically significant difference between staurosporine 200 nM and all other treatments ($P < .001$), 50 μM hydrogen peroxide (H_2O_2) vs. negative control ($P = .031$), and harmame 250 μM vs. negative control and harmame 50 μM ($P < .01$).

The difference between cultures was significant in both tests (apoptosis and necrosis), but the treatment affected all cultures at the same levels; in other words, the increase in necrosis and apoptosis was related to the increased concentration of harmame; both for apoptosis and necrosis, staurosporine 200 nM was a good positive control (with a much higher effect on apoptosis than on necrosis), while 50 μM H_2O_2 was not.

4. Discussion

β CAs, including harmame, occur in several medicinal plants and dietary components. They have many biological properties, including neurological effects, and these activities explain the use of medicinal plants containing β CAs in traditional Chinese medicine and other traditional medicine. Lately, harmame has been incriminated in the pathogenesis of ET; however, there have been few studies on that matter and little is known about a possible association, which drew our attention to the need to develop a reliable *in vitro* model to study the neurotoxicity of harmame and other chemical molecules distributed in the environment and medicinal plants.⁷⁰

The 3D cell cultures and organoids are being growingly used to bridge the gap between *in vitro* 2D cell cultures and *in vivo* animal models. There is a consensus that 3D models are more physiologically relevant than biochemical assays and 2D cell cultures, as they more closely represent the microenvironment, cell-to-cell interactions, and biological processes that occur *in vivo*.^{61–63} However, the 3D neuronal cultures remain challenging in many technical aspects. Notably, the sizes of these 3D spheroids must be controlled because of the lack of circulatory system, which may cause central necrosis zones due to a lack of oxygen and nutrients.

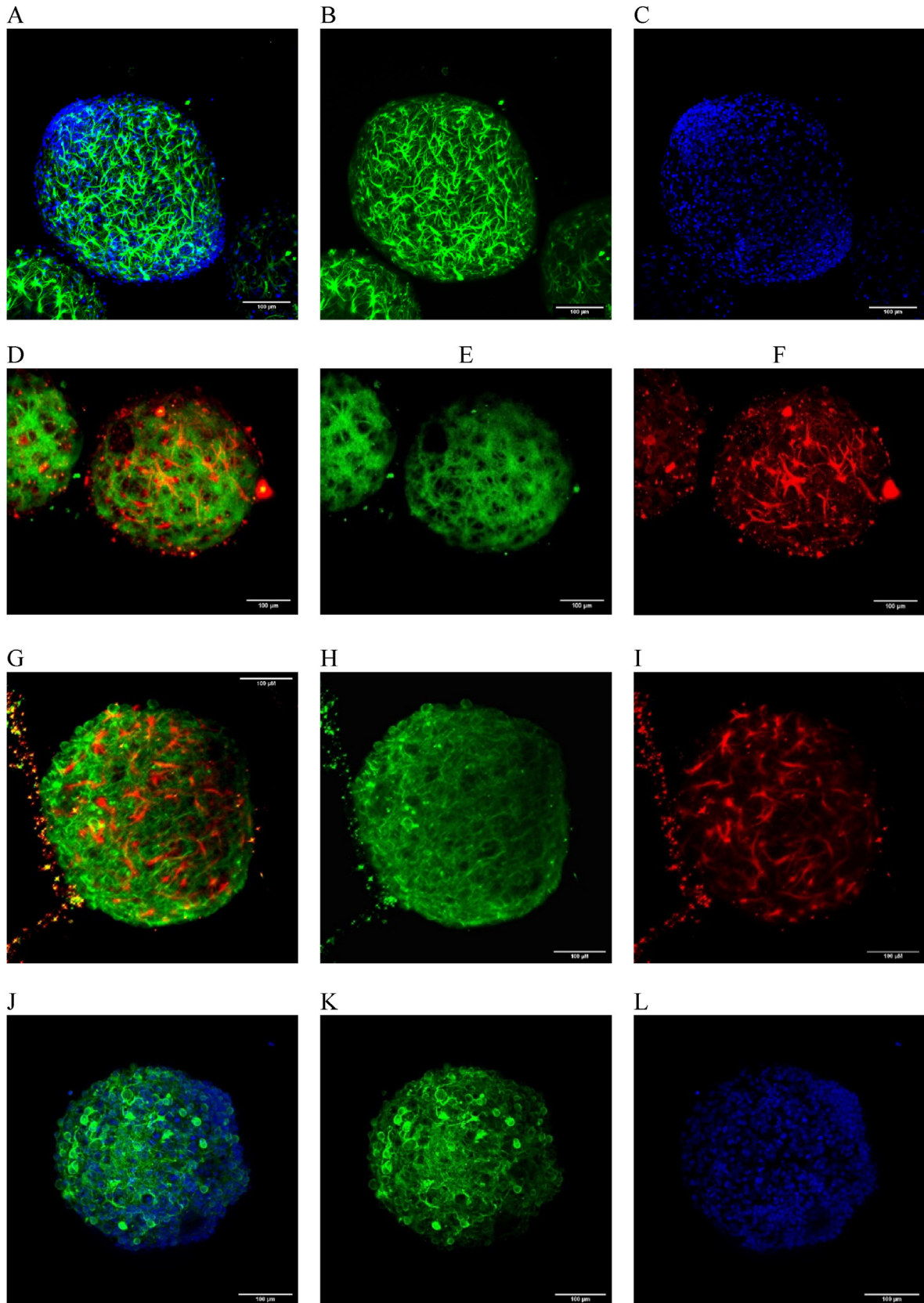


Fig. 10. Confocal images on day 14 indicate that the neural spheroids contain different CNS cell types, including (A) GFAP + DAPI, (B) GFAP, (C) DAPI, (D) GFAP + Tau, (E) Tau, (F) GFAP, (G) MAP2 + Iba-1, (H) Iba-1, (I) MAP2, (J) Class III β -tubulin + DAPI, (K) class III β -tubulin, (L) DAPI (TUB).
Notes: DAPI: 4',6-diamidino-2-phenylindole; MAP2: microtubule-associated protein 2; GFAP: glial fibrillary acidic protein. Magnification: $20\times$. Scale bar = 100 μm .

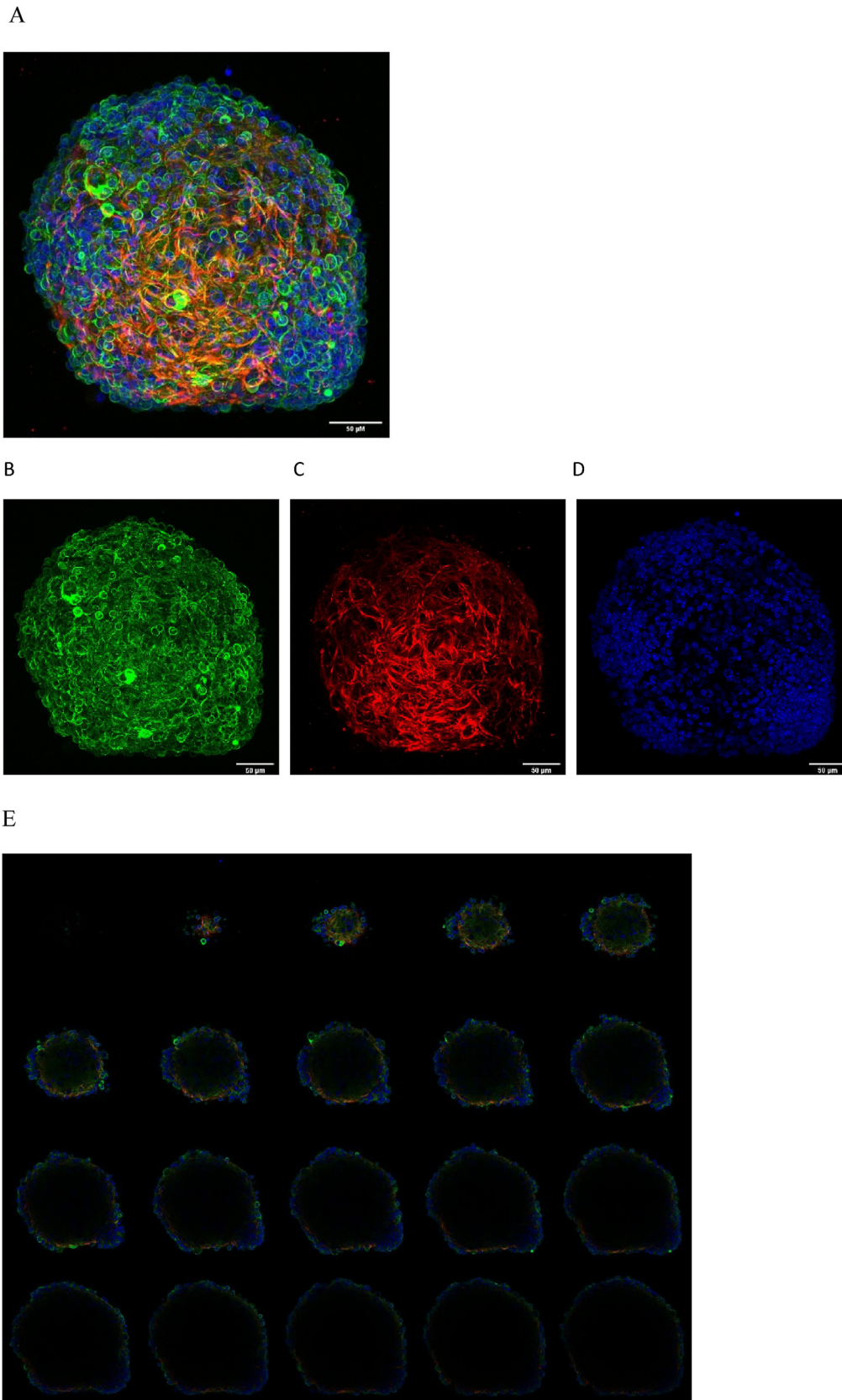


Fig. 11. Confocal images obtained with a water immersion on day 14: (A) the different types of cells in neural spheroids, including (B) neurons (class III β -tubulin, green), (C) astrocytes (GFAP, red), and (D) nuclei (DAPI, blue); (E) the 20 stacks of the composite image presented above illustrate the dark center, indicating the challenges to high-quality deep imaging within a 3D spheroid.

Notes: Magnification: $40\times$. Scale bar = $50\ \mu\text{m}$.

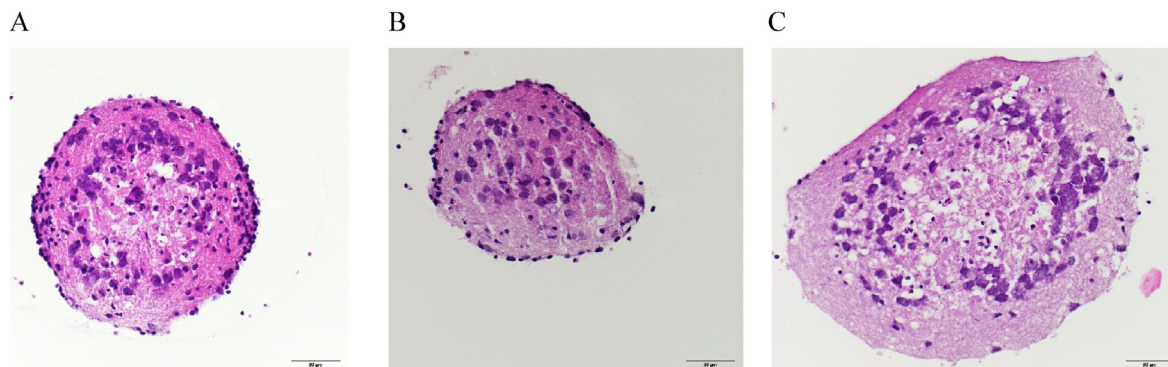


Fig. 12. Visible light images for different slices of 14 DIV neuronal spheroids: (A) and (B) at 100 μm depth, while (C) at 200 μm , stained with H&E staining.

Notes: Cell nuclei are colored in shades of blue and purple, and connective tissue is colored in shades of pink. The center of spheroids contains cells but a lower number, and their cell bodies are larger than those in the periphery. The extracellular matrix is denser in the periphery than in the center. Magnification: $40\times$. Scale bar = 50 μm .

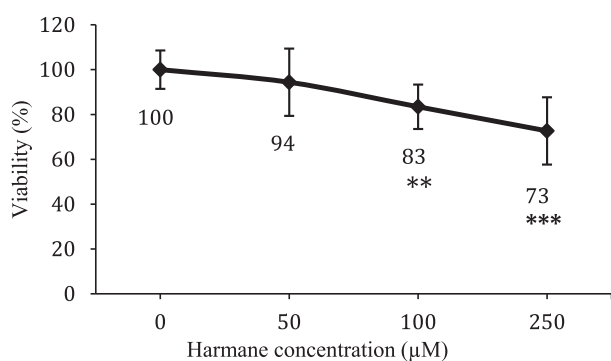


Fig. 13. Cell viability after 24 h exposure to different concentrations of harmaline.

Notes: Data from 6 biologically independent experiments performed with 3 technical replicates (resazurin viability test). There is a clear trend in viability reduction with harmaline concentration. There is a statistically significant difference between the negative control and harmaline 100 and 250 μM concentrations (ANOVA test). ** $P = .006$, *** $P < .001$. $n = 18$.

This limitation is a key point in the development of 3D neural spheroids as it may jeopardize the sensitivity of toxicity screening tests.⁷¹ To circumvent these problems, advanced culture techniques based on growing neurons either in microfluidic circuitry⁷² or in co-culture with blood capillaries⁷³ have been proposed; these are, however, much more technically challenging. Involved technologies are also proposed for high-throughput workflow, accuracy, precision, culture manipulation, and integrity. However, such methods are still largely artistic, not standardized, and not accessible in all laboratories.⁷⁴

In this study, we described a reproducible 3D neurosphere culture based on a non-scaffold technique, which requires reasonable laboratory equipment, using prenatal mouse neural cells and agarose-molded wells. Although this method requires simple laboratory equipment, it needs a very careful and precise experimenter as different factors affect the quality and quantity of spheroids, starting from the set-up prior to culture and ending by spheroid harvest, as follows: (1) the quality of agarose micro-well shapes affects the distribution of cells and thus the diameter of spheroids; (2) the pre-culture equilibration with the medium t ; (3) the dissection and dissociation of cortical tissues influence the quality of neurons seeded; (4) the time needed for the cells to settle and aggregate before adding the total volume of medium; (5) and the regular and timely medium renewal.

We developed our method by testing different microwell diameters and cell densities, and the diameter was controlled by altering the number of seeded cells. Our 3D neurosphere cultures comprised all brain cell types, including glial, microglial, and neural cells. Moreover, the quantitative fluorescence intensities corresponding to the different markers were invariable between the cultures, demonstrating high reproducibility in terms of the proportions of cell types in spheroids.

Quantifying the fluorescence of spheroids is challenging and needs optimization and attention to increase the robustness of assays and compatibility with high-throughput screening. In 2D cell cultures, the signals are typically normalized based on the field of view or numbers of cells; neither of the approaches is applicable in spheroids, for which the method of fluorescence signals normalization must reflect the variables of width, length, and height radii of the spheroids.⁷⁵ In our work, the attention to the staining methods, their optimization, and normalization of the fluorescence signals were taken into consideration to reduce the errors and enhance sensitivity. The duration of spheroid staining was increased; the signal was normalized by eliminating the size-based differences in fluorescence; and, to do so, we analyzed the spheroids within narrow ranges of radii. Although applying flow cytometry analysis would undoubtedly be more precise for the quantification of cell types, our trials indicated that it is quite challenging to properly dissociate a neurosphere.

Confocal microscopy provides the highest sensitivity and X, Y, and Z resolution imaging with high-throughput data acquisition. Still, the imaging of 3D neural spheroids remains challenging in the following aspects: (1) the inability of imaging optics to penetrate deep into the 3D structure to provide relevant information (light scattering and absorption limit confocal imaging at depths around 100 μm); (2) the density and diameter of the 3D spheres remain key parameters for accessibility to imaging optics; (3) further challenge remains in the measurement (segmentation and quantification) of relevant 3D parameters in the reconstituted images, if possible in a medium- to high-throughput manner.⁷⁶

The use of some techniques allowed us to improve confocal imaging. Namely, we used a water immersion objective, which improved the resolution as its higher numerical aperture allowed to capture more light and smaller focal depth reduced the background light and light scattering compared with air objectives; optical clearing techniques were used to remove the lipid and protein molecules that contribute to light scattering effects, and thus homogenize refractive indices within spheroids.⁷⁷ We applied these 2 techniques to enable fluorescent imaging deep within the sphere. The obtained confocal spheroid images enlightened the complexity

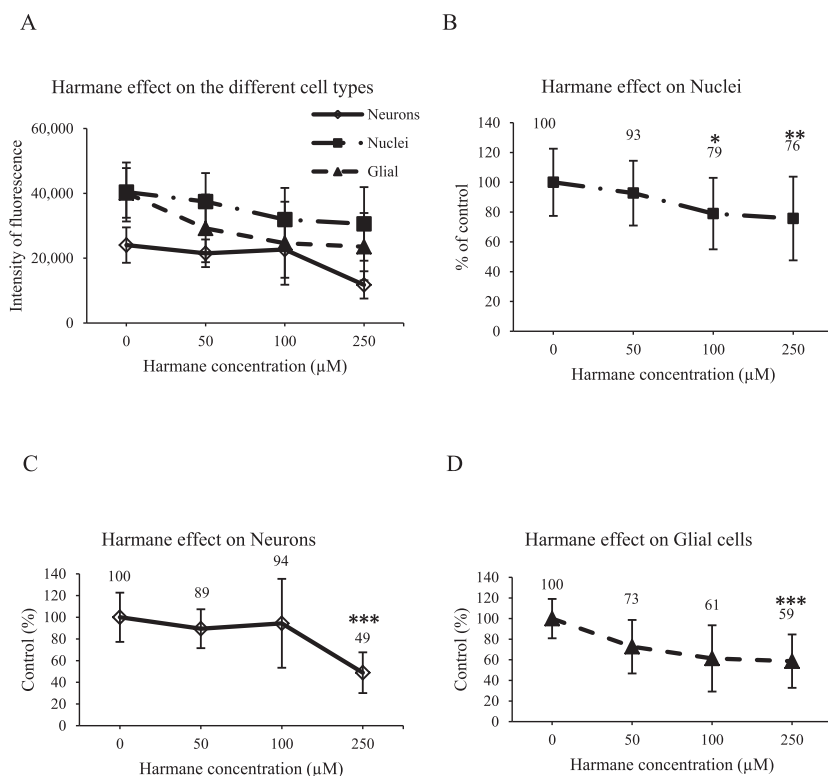


Fig. 14. Fluorescence intensities after 24 h exposure to different concentrations of harmane. (A) absolute fluorescence intensities; there is a clear trend in reduction with the higher harmane concentrations; (B) fluorescence of DAPI (nuclei), relative to the control condition; there was a statistically significant difference between the control group and harmane 100 and 250 μM groups ($P = .01$ and $.002$, respectively); (C) fluorescence of MAP2 (neurons), relative to the control condition; there was a statistically significant difference for all groups vs. harmane 250 μM ($P < .001$); (D) fluorescence of GFAP (glial cells), relative to the control condition; the difference was statistically significant for all groups vs. harmane 250 μM ($P < .001$).

Notes: Data from 3 biologically independent experiments performed with 3 technical replicates (mean \pm SD). $n = 12$.

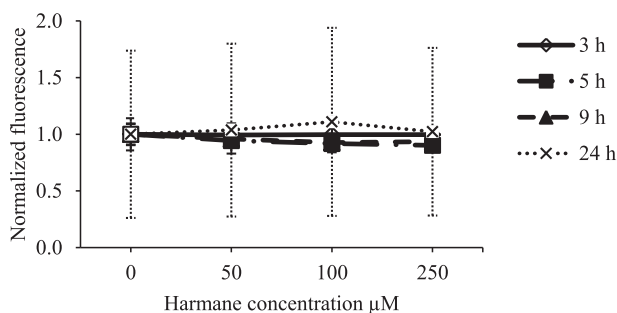


Fig. 15. ROS production measured with a DCFH test after 3, 5, 9, and 24 h of exposure to different concentrations of harmane (0, 50, 100, 250 μM).

Notes: Data from 3 biologically independent experiments performed with 3 technical replicates (mean \pm SD). The difference was not statistically significant for the different treatments and at the different time points. $n = 9$.

of the structure and illustrated the intricate architecture of the spheroids' microenvironment with the highest sensitivity.

Nevertheless, the limited penetration depth raises the question about cell viability in the center of spheroids, which appears dark in confocal images. In addition, analyzing confocal images, e.g., for measuring connections, axons, or dendrites sizes, remains complex and requires further expertise.

To visualize the spheroid's centers, we applied traditional histological embedding, sectioning, and staining⁷⁸ with H&E staining to

highlight a broad range of cytoplasmic, nuclear, and extracellular matrix features. The observation of multiple H&E stained histological slices at different depths of spheroids, including the center, indicated that the dark centers were due to the light penetration issue, and that necrosis was limited. Compared with the rest of the spheroid, the center appeared to contain more connective tissue and fewer cells. This slicing technique might be the best to analyze the complexity of the spheroids and could be completed by staining the slices with different antibodies. However, this method certainly reduces the analytical throughput and the advantages of 3D imaging.

For the cytotoxicity and ROS assays, we used harmane as a test compound at different concentrations, over 24 h. Harmane, a natural β CA, is described as both a neurotoxic and a neuroprotective molecule. It is notably a strong inhibitor of myeloperoxidase⁷⁹—a key player in neuroinflammation⁸⁰—a monoamine oxidase inhibitor⁸¹, an antioxidant, and a chemoprotective agent.⁸² The neurotoxicity of harmane has been related to its dopaminergic effects.⁸³ However, harmane has been incriminated in the pathogenesis of ET.⁸⁴

The "resazurin reduction test" is considered a simple method for measuring cell proliferation and cytotoxicity that can be quantified by spectrophotometry of the culture medium. The application of this test on 3D spheroids raises a question of whether the cell-to-cell interaction inhibits resazurin uptake and reduces the reduction activity.⁸⁵ For that, we applied a verification method for the test, by comparing the resazurin measures of viability with the measure of neurons (MAP2), glial cells (GFAP), and nuclei (DAPI) fluorescence. The resazurin assay indicated a harmane concentration-based trend in spheroids viability decrease after 24 h, with a reduction significant at 100 and 250 μM. Moreover, the

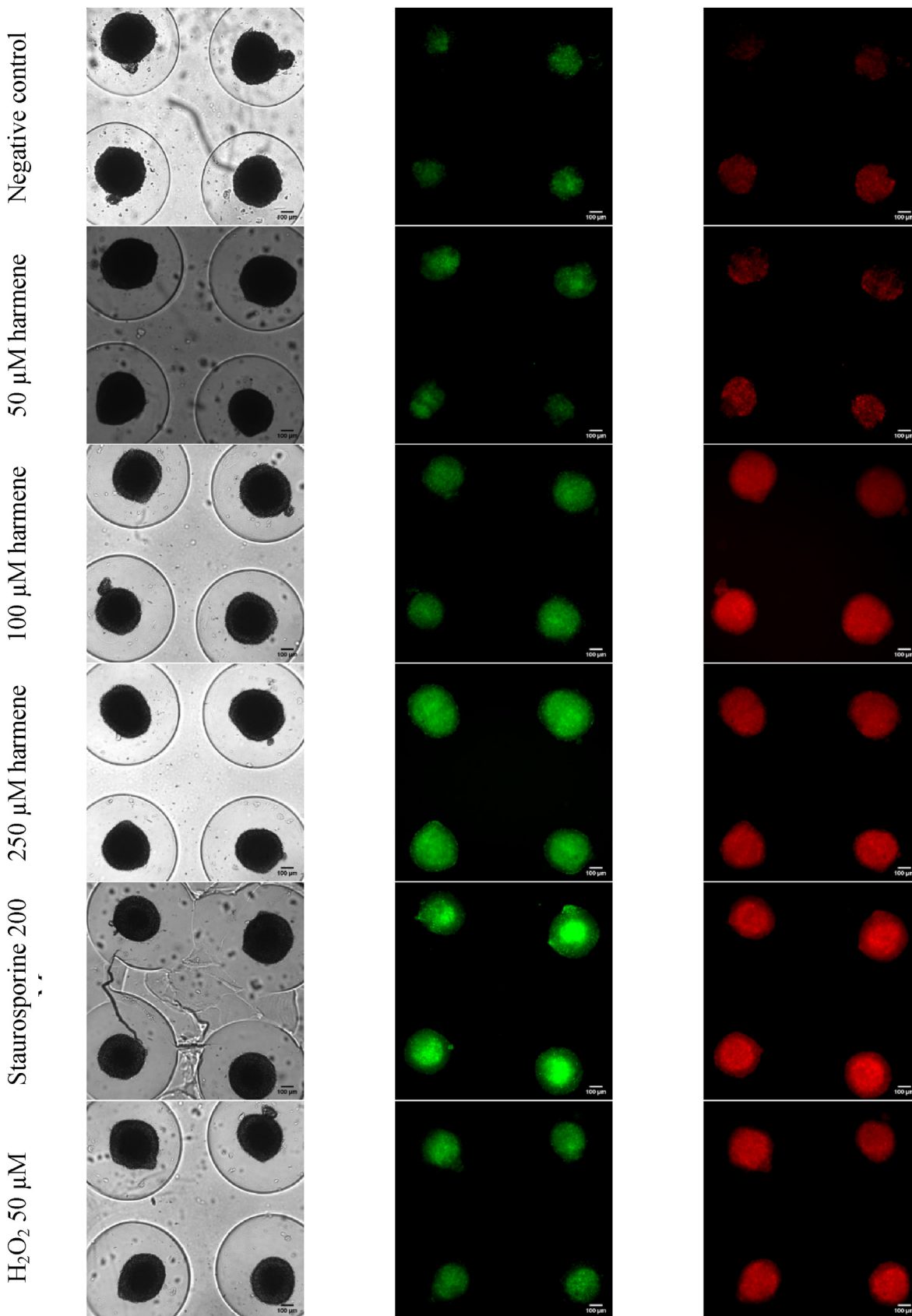


Fig. 16. Phase-contrast and fluorescence microscopy images of neuronal spheroids after exposure to different harmene concentrations (0, 50, 100, and 250 μM), staurosporine 200 nM, and 50 μM H_2O_2 .

Notes: The phase-contrast images were used to define the acceptable spheroids; caspases 3/7 in apoptotic cells induce a green fluorescence, while propidium iodide stains nucleic acids in necrotic cells with red fluorescence. Magnification: $10\times$. Scale bar = 100 μm .

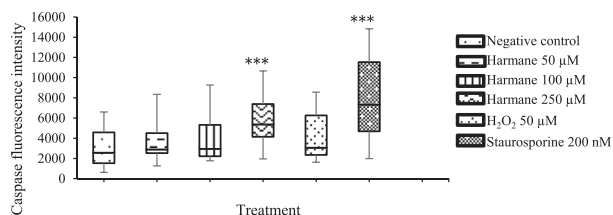


Fig. 17. The caspase-induced fluorescence intensity after 24 h exposure to different concentrations of harmane, staurosporine, and H_2O_2 .

Notes: Data from 3 biologically independent experiments performed with 3 technical replicates. Bar in the box represents the median of data. Number of measured spheroids: 35 negative controls, 35 harmane 50 μM , 42 harmane 100 μM , 32 harmane 250 μM , 44 H_2O_2 , 41 staurosporine. There was a statistically significant difference between the negative control and both harmane 250 μM and staurosporine 200 nM groups ($P < .001$).

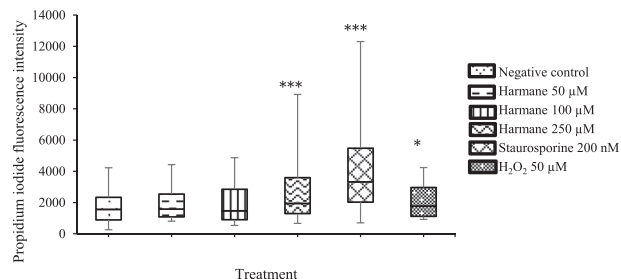


Fig. 18. The propidium iodide fluorescence intensity after 24 h exposure to different concentrations of harmane, staurosporine, and H_2O_2 .

Notes: Data from 3 biologically independent experiments performed with 3 technical replicates. Number of measured spheroids: 35 control negative, 35 harmane 50 μM , 42 harmane 100 μM , 32 harmane 250 μM , 44 H_2O_2 , 41 staurosporine. There was a statistically significant difference between the negative control and harmane 250 μM ($P < .001$), staurosporine 200 nM ($P < .001$), and H_2O_2 ($P = .03$).

measurement of intensity fluorescence for neurons, glia, and nuclei in spheroids exposed to different concentrations of harmane indicated a similar reduction in viability, particularly for DAPI. These results confirm the neurotoxic effect of harmane and the suitability of a simple resazurin assay to measure the cell viability in spheroids.

Next, DCFH assay was selected for extracellular ROS analysis. The leaked ROS measurement indicated no significant difference between the control conditions and the different harmane treatments, at the different incubation times tested (up to 24 h).

The reduction in viability with harmane demands to analyze whether the cytotoxicity is due to an apoptotic or necrotic effect; apoptosis is an active cell death mechanism, programmed and related to internal cellular factors, while necrosis is a passive death, uncontrolled and dependent on extracellular factors.⁸⁶ To investigate an eventual apoptotic role of harmane, we measured the caspase cascade, that is, the fluorescence intensity generated by the cleavage of a caspase 3/7 substrate (positive control, staurosporine 200 nM); caspases are proteases and some of them are involved in apoptosis. We also determined an eventual necrotic effect by a propidium iodide test (positive control, H_2O_2 50 μM); this fluorophore can stain the DNA of necrotic cells and cells with damaged membrane. Both tests require fluorescence measurement, with

normalization of the fluorescence intensity to the spheroid diameter, carefully delineating the measurement area by hand.

On the one hand, staurosporine is clearly a proapoptotic agent, but some of the cells were also stained with propidium iodide; spheroids appeared quite resistant to H_2O_2 , which yielded only a weak necrotic effect. In 2D neuronal cultures, H_2O_2 concentration typically yields 50% of necrotic cell death after incubation of 12 h.⁸⁷ This observation might relate to the selectively toxic effect of H_2O_2 on immature neurons culture (6 DIV) compared with mature neurons culture (20 DIV).⁸⁸ This may be worthy of further investigation for eventual survival mechanisms as this type of resistance may question the relevance of data obtained on 2D cultures. On the other hand, it is possible that the toxicant is not evenly distributed within the spheroid, biasing the concentrations to which cells are really exposed. The tests indicated that harmane has both apoptotic and necrotic effects, with a probable predominance of necrosis. As fluorescence measurements are quite challenging, yielding a high heterogeneity of data, it would be advantageous to use another method such as flow cytometry; however, despite our efforts, we did not manage to successfully apply flow cytometry on spheroids due to problems of cell dissociation.

5. Conclusion

Reducing the number of animals that are used in research is very demanding and requires better *in vitro* systems. Indeed, the classically used 2D cultures do not meet all the researchers' needs as they do not represent the real *in vivo* environment in which cells spatially and chemically interact; their lack of predictivity increases the cost and failure rate of clinical trials and this is especially the case in neurosciences. Recently, 3D cell cultures have received much attention, as these are closer to tissue models; they are being used growingly in the hope to bridge the gap between *in vitro* 2D cell cultures and *in vivo* animal models. There is a consensus that 3D models are physiologically relevant, as they more closely represent the microenvironments, cell-to-cell interactions, and biological processes that occur *in vivo*. Still, the challenges with 3D models reside in end-point measurements.

The 3D neurosphere culture presented in this work has shown the ability to reproduce a 3D culture using simple materials and routine laboratory equipment. Despite the challenges in 3D culture and data obtaining, this 3D neurosphere model mimics a neuronal microenvironment, allowing a fine study of neurodegenerative disorders and the effect of chemicals on the brain. However, we raise the question as to whether an animal source of cells is the best model, especially for CNS diseases, considering the complexity of the brain in humans compared with rodents. It would be interesting to investigate 3D models based on human stem cells, which may be more relevant to diseases such as ET, where genetic factors play a role; this could upgrade the research to another level.

Harmane was tested in our neural spheroid model for cytotoxicity and oxidative stress induction. The obtained results support the role of harmane as a neurotoxic agent but at a high concentration; our data do not support a possible neuroprotective role of harmane. Further studies are required to elucidate the biological activities of harmane and to decipher, via *in vitro* tests, an eventual relationship with ET disorder. Further research is needed to determine the causes and consequences of elevated blood concentrations of harmane shown in ET patients.

Funding

This research was in part funded through a Fonds Medical pour la Recherche dans le Hainaut (FMRH) grant and a Kangaroo grant from the UMONS Health Institute.

CRedit authorship contribution statement

Rania Aro: Conceptualization, methodology, data curation, writing – original draft, and writing – review & editing. **Amandine Nachtergaeel:** resources, and data curation. **Laurence Ris:** Conceptualization, methodology, supervision, and funding acquisition. **Mario Manto:** Conceptualization, and methodology. **Pierre Duez:** Conceptualization, methodology, writing – review & editing, supervision, and funding acquisition.

Declaration of competing interest

The authors declare that they have no competing interests.

Acknowledgments

We thank Dr. Alpha Diallo, Dr. Marvyn Pichueque, Dr. Mathilde Wauters, Charles Poteau, Claudio Palmieri, the Centre for Microscopy and Molecular Imaging (CMMI), and Biology of Marine Organisms and Biomimetics Unit of UMONS for their support.

References

- Barbosa DJ, Capela JP, de Lourdes Bastos M, Carvalho F. *In vitro* models for neurotoxicology research. *Toxicol Res.* 2015;4(4):801–842.
- Vajda FJ. Neuroprotection and neurodegenerative disease. *J Clin Neurosci.* 2002;9(1):4–8.
- Duval K, Grover H, Han LH, et al. Modeling physiological events in 2D vs. 3D cell culture. *Physiology.* 2017;32(4):266–277.
- Bonnier F, Keating ME, Wrobel TP, et al. Cell viability assessment using the Alamar blue assay: a comparison of 2D and 3D cell culture models. *Toxicol Vitro.* 2015;29(1):124–131.
- Baker BM, Chen CS. Deconstructing the third dimension – how 3D culture microenvironments alter cellular cues. *J Cell Sci.* 2012;125(13):3015–3024.
- Lee J, Cuddihy MJ, Kotov NA. Three-dimensional cell culture matrices: state of the art. *Tissue Eng B Rev.* 2008;14(1):61–86.
- Huang G, Li F, Zhao X, et al. Functional and biomimetic materials for engineering of the three-dimensional cell microenvironment. *Chem Rev.* 2017;117(20):12764–12850.
- Birgersdotter A, Sandberg R, Ernberg I. Gene expression perturbation *in vitro*—a growing case for three-dimensional (3D) culture systems. *Semin Cancer Biol.* 2005;15(5):405–412.
- Bhadriraju K, Chen CS. Engineering cellular microenvironments to improve cell-based drug testing. *Drug Discov Today.* 2002;7(11):612–620.
- Zietarska M, Maugard CM, Filali-Mouhim A, et al. Molecular description of a 3D *in vitro* model for the study of epithelial ovarian cancer (EOC). *Mol Carcinog.* 2007;46(10):872–885.
- Benton JA, Fairbanks BD, Anseth KS. Characterization of valvular interstitial cell function in three dimensional matrix metalloproteinase degradable PEG hydrogels. *Biomaterials.* 2009;30(34):6593–6603.
- Bi YA, Kazolias D, Duignan DB. Use of cryopreserved human hepatocytes in sandwich culture to measure hepatobiliary transport. *Drug Metab Dispos.* 2006;34(9):1658–1665.
- Lancaster MA, Renner M, Martin CA, et al. Cerebral organoids model human brain development and microcephaly. *Nature.* 2013;501(7467):373–379.
- Beauchamp P, Moritz W, Kelm JM, et al. Development and characterization of a scaffold-free 3D spheroid model of induced pluripotent stem cell-derived human cardiomyocytes. *Tissue Eng C Methods.* 2015;21(8):852–861.
- Suga H, Kadoshima T, Minaguchi M, et al. Self-formation of functional adenyphypophysis in three-dimensional culture. *Nature.* 2011;480(7375):57–62.
- Nakano T, Ando S, Takata N, et al. Self-formation of optic cups and storable stratified neural retina from human ESCs. *Cell Stem Cell.* 2012;10(6):771–785.
- Sato T, Vries RG, Snippert HJ, et al. Single Lgr5 stem cells build crypt-villus structures *in vitro* without a mesenchymal niche. *Nature.* 2009;459(7244):262–265.
- Zanoni MPF, Arienti C, Zamagni A, et al. 3D tumor spheroid models for *in vitro* therapeutic screening: a systematic approach to enhance the biological relevance of data obtained. *Sci Rep.* 2016;6:19103.
- Lee J, Lilly GD, Doty RC, Podsiadlo P, Kotov NA. *In vitro* toxicity testing of nanoparticles in 3D cell culture. *Small.* 2009;5(10):1213–1221.
- Otieno MA, Gan J, Proctor W. *Drug-Induced Liver Toxicity.* New York, USA: Springer New York; 2018.
- Kuo CT, Wang JY, Lin YF, Wo AM, Chen BPC, Lee H. Three-dimensional spheroid culture targeting versatile tissue bioassays using a PDMS-based hanging drop array. *Sci Rep.* 2017;7(1):4363.
- Iskandar AR, Xiang Y, Frentzel S, et al. Impact Assessment of cigarette smoke exposure on organotypic bronchial epithelial tissue cultures: a comparison of mono-culture and coculture model containing fibroblasts. *Toxicol Sci.* 2015;147(1):207–221.
- Barros AS, Costa EC, Nunes AS, de Melo-Diogo D, Correia IJ. Comparative study of the therapeutic effect of Doxorubicin and Resveratrol combination on 2D and 3D (spheroids) cell culture models. *Int J Pharm.* 2018;551(1):76–83.
- Balmana M, Diniz F, Feijão T, Barrias CC, Mereiter S, Reis CA. Analysis of the effect of increased α 2,3-sialylation on RTK activation in MKN45 gastric cancer spheroids treated with crizotinib. *Int J Mol Sci.* 2020;21(3):722.
- van Duinen V, Trietsch SJ, Joore J, Vulto P, Hankemeier T. Microfluidic 3D cell culture: from tools to tissue models. *Curr Opin Biotechnol.* 2015;35:118–126.
- Cushing MC, Anseth KS. Materials science. Hydrogel cell cultures. *Science.* 2007;316(5828):1133–1134.
- Chen X, Ergun A, Gevgilili H, Ozkan S, Kalyon DM, Wang H. Shell-core bilayered scaffolds for engineering of vascularized osteon-like structures. *Biomaterials.* 2013;34(33):8203–8212.
- Dhiman HK, Ray AR, Panda AK. Three-dimensional chitosan scaffold-based MCF-7 cell culture for the determination of the cytotoxicity of tamoxifen. *Biomaterials.* 2005;26(9):979–986.
- Elias Volkmer ID, Sven O, Achim S, et al. Hypoxia in static and dynamic 3D culture systems for tissue engineering of bone. *Tissue Eng Part A.* 2008;14(8):1331–1340.
- Li L, LaBarbera DV. *Comprehensive Medicinal Chemistry III.* Amsterdam, Netherlands: Elsevier; 2017.
- Astashkina A, Grainger DW. Critical analysis of 3-D organoid *in vitro* cell culture models for high-throughput drug candidate toxicity assessments. *Adv Drug Deliv Rev.* 2014;69–70:1–18.
- Pereira S, Coutinho D, Matos A, Silva W, Fabrino D. Three-dimensional cell culture, opportunities and challenges for bioprocess engineers. *Braz J Biol Sci.* 2016;3:263–277.
- Jankovic J. Essential tremor: clinical characteristics. *Neurology.* 2000;54(11):S21–S25.
- Brennan KC, Jurewicz EC, Ford B, Pullman SL, Louis ED. Is essential tremor predominantly a kinetic or a postural tremor? A clinical and electrophysiological study. *Mov Disord.* 2002;17(2):313–316.
- Lavita SI, Aro R, Kiss B, Manto M, Duez P. The role of beta-carboline alkaloids in the pathogenesis of essential tremor. *Cerebellum.* 2016;15(3):276–284.
- Louis ED. Environmental epidemiology of essential tremor. *Neuroepidemiology.* 2008;31(3):139–149.
- Seidl SE, Santiago JA, Bilyk H, Potashkin JA. The emerging role of nutrition in Parkinson's disease. *Front Aging Neurosci.* 2014;6:36.
- Gomez-Pinilla F, Gomez AG. The influence of dietary factors in central nervous system plasticity and injury recovery. *Pharm Manag PM R.* 2011;3(6):S111–S116.
- Brandt J. Diet in brain health and neurological disorders: risk factors and treatments. *Brain Sci.* 2019;9:234.
- Ong YL, Deng X, Tan EK. Etiological links between environmental and lifestyle factors and essential tremor. *Ann Clin Transl Neurol.* 2019;6(5):979–989.
- Louis ED, Zheng W. Beta-carboline alkaloids and essential tremor: exploring the environmental determinants of one of the most prevalent neurological diseases. *Sci World J.* 2010;10:1783–1794.
- Louis ED, Factor-Litvak P, Liu X, et al. Elevated brain harmaline (1-methyl-9H-pyrido[3,4-b]indole) in essential tremor cases vs. controls. *Neurotoxicology.* 2013;38:131–135.
- Higgins D, Burack M, Lein P, Banker G. Mechanisms of neuronal polarity. *Curr Opin Neurobiol.* 1997;7(5):599–604.
- Kolasiewicz W, Kuter K, Wardas J, Ossowska K. Role of the metabotropic glutamate receptor subtype 1 in the harmaline-induced tremor in rats. *J Neural Transm.* 2009;116(9):1059–1063.
- Louis ED, Keating GA, Bogen KT, Rios E, Pellegrino KM, Factor-Litvak P. Dietary epidemiology of essential tremor: meat consumption and meat cooking practices. *Neuroepidemiology.* 2008;30(3):161–166.
- Li S, Liu W, Teng L, Cheng X, Wang Z, Wang C. Metabolites identification of harmaline *in vitro/in vivo* in rats by ultra-performance liquid chromatography combined with electrospray ionization quadrupole time-of-flight tandem mass spectrometry. *J Pharm Biomed Anal.* 2014;92:53–62.
- Monsef HR, Ghobadi A, Iranshahi M, Abdollahi M. Antinociceptive effects of Peganum harmala L. alkaloid extract on mouse formalin test. *J Pharm Pharmacol Sci.* 2004;7(1):65–69.
- Farouk L, Laroubi A, Aboufatima R, Benharref A, Chait A. Evaluation of the analgesic effect of alkaloid extract of Peganum harmala L.: possible mechanisms involved. *J Ethnopharmacol.* 2008;115(3):449–454.
- Pathan A. Peganum harmala: a phyto-pharmacological review. *Inventi Rapid Planta Activa.* 2012;4:1–2.
- Li S, Teng L, Liu W, et al. Pharmacokinetic study of harmaline and its 10 metabolites in rat after intravenous and oral administration by UPLC-ESI-MS/MS. *Pharm Biol.* 2016;54(9):1768–1781.
- Zhu W, Du Y, Meng H, Dong Y, Li L. A review of traditional pharmacological uses, phytochemistry, and pharmacological activities of Tribulus terrestris. *Chem Cent J.* 2017;11(1):60.
- Harris AC, Muelken P, LeSage MG. β -Carbolines found in cigarette smoke elevate intracranial self-stimulation thresholds in rats. *Pharmacol Biochem Behav.* 2020;198(173041):11.
- Rommelspacher HA-ML, Kostrzewa RM, Arche T. *Isoquinolines and Beta-Carbolines as Neurotoxins and Neuroprotectants.* Boston, USA: Springer; 2012.
- Koleva II, van Beek TA, Soffers AE, Dusemund B, Rietjens IM. Alkaloids in the human food chain—natural occurrence and possible adverse effects. *Mol Nutr Food Res.* 2012;56(1):30–52.

55. Matsubara K, Gonda T, Sawada H, et al. Endogenously occurring beta-carboline induces parkinsonism in nonprimate animals: a possible causative protoxin in idiopathic Parkinson's disease. *J Neurochem*. 1998;70(2):727–735.
56. Wernicke C, Hellmann J, Zięba B, et al. 9-Methyl- β -carboline has restorative effects in an animal model of Parkinson's disease. *Pharmacol Rep*. 2010;62(1):35–53.
57. Herraiz T, Chaparro C. Human monoamine oxidase is inhibited by tobacco smoke: beta-carboline alkaloids act as potent and reversible inhibitors. *Biochem Biophys Res Commun*. 2005;326(2):378–386.
58. Scott WK, Zhang F, Stajich JM, Scott BL, Stacy MA, Vance JM. Family-based case-control study of cigarette smoking and Parkinson disease. *Neurology*. 2005;64(3):442–447.
59. Emerit J, Edeas M, Bricaire F. Neurodegenerative diseases and oxidative stress. *Biomed Pharmacother*. 2004;58(1):39–46.
60. Cataldo JK, Prochaska JJ, Glantz SA. Cigarette smoking is a risk factor for Alzheimer's disease: an analysis controlling for tobacco industry affiliation. *J Alzheimers Dis*. 2010;19(2):465–480.
61. Edmondson R, Broglie JJ, Adcock AF, Yang L. Three-dimensional cell culture systems and their applications in drug discovery and cell-based biosensors. *Assay Drug Dev Technol*. 2014;12(4):207–218.
62. Ravi M, Paramesh V, Kaviya SR, Anuradha E, Solomon FDP. 3D cell culture systems: advantages and applications. *J Cell Physiol*. 2015;230(1):16–26.
63. Elliott NT, Yuan F. A review of three-dimensional *in vitro* tissue models for drug discovery and transport studies. *J Pharmacol Sci*. 2011;100(1):59–74.
64. Dingle YTL, Boutin ME, Chirila AM, et al. Three-dimensional neural spheroid culture: an *in vitro* model for cortical studies. *Tissue Eng C Methods*. 2015;21(12):1274–1283.
65. MicroTissues Inc. Casting, equilibrating and seeding the 3D Petri Dish®. Available at <https://www.microtissues.com/protocols>. Accessed November 1, 2021.
66. Pamies D, Block K, Lau P, et al. Rotenone exerts developmental neurotoxicity in a human brain spheroid model. *Toxicol Appl Pharmacol*. 2018;354:101–114.
67. Bunel V, Ouedraogo M, Nguyen AT, Stévinny C, Duez P. Methods applied to the *in vitro* primary toxicology testing of natural products: state of the art, strengths, and limits. *Planta Med*. 2014;80(14):1210–1226.
68. Silveira LR, Pereira-Da-Silva L, Juel C, Hellsten Y. Formation of hydrogen peroxide and nitric oxide in rat skeletal muscle cells during contractions. *Free Radic Biol Med*. 2003;35(5):455–464.
69. Cathcart R, Schwiers E, Ames BN. Detection of picomole levels of hydroperoxides using a fluorescent dichlorofluorescein assay. *Anal Biochem*. 1983;134(1):111–116.
70. Aro R, Duez P, Nachtergaeel A, Manto M. Hampering Essential Tremor Neurodegeneration in Essential Tremor: Present and Future Directions. *Frontiers in clinical drug research – CNS and neurological disorders. Sharjah United Arab Emirates;Bentham science*. 2019;7:1–32.
71. Barisam M, Saidi M, Kashaninejad N, Nguyen NT. Prediction of necrotic core and hypoxic zone of multicellular spheroids in a microbio-reactor with a U-shaped barrier. *Micromachines*. 2018;9(3):94.
72. Li XJ, Valadez AV, Zuo P, Nie Z. Microfluidic 3D cell culture: potential application for tissue-based bioassays. *Bioanalysis*. 2012;4(12):1509–1525.
73. Osaki T, Sivathanu V, Kamm RD. Engineered 3D vascular and neuronal networks in a microfluidic platform. *Sci Rep*. 2018;8(1):5168.
74. Kriston-Vizi J, Flotow H. Getting the whole picture: high content screening using three-dimensional cellular model systems and whole animal assays. *Cytometry A*. 2017;91(2):152–159.
75. Leary E, Rhee C, Wilks B, Morgan JR. Accurate quantitative wide-field fluorescence microscopy of 3D spheroids. *Biotechniques*. 2016;61(5):237–247.
76. Boutin ME, Voss TC, Titus SA, Cruz-Gutierrez K, Michael S, Ferrer M. A high-throughput imaging and nuclear segmentation analysis protocol for cleared 3D culture models. *Sci Rep*. 2018;8(1):11135.
77. Graf BW, Boppert SA. Imaging and analysis of three-dimensional cell culture models. *Methods Mol Biol*. 2010;591:211–227.
78. Gabriel J, Brennan D, Elisseeff JH, Beachley V. Microarray embedding/sectioning for parallel analysis of 3D cell spheroids. *Sci Rep*. 2019;9(1):16287.
79. Bensalem S, Soubhye J, Aldib I, et al. Inhibition of myeloperoxidase activity by the alkaloids of *Peganum harmala* L. (Zygophyllaceae). *J Ethnopharmacol*. 2014;154(2):361–369.
80. Aricioglu F, Arkan G, Kandemir C, Sirvanci S, Ozkartal C, Utkan T. Harmane suppresses microglial neuroinflammatory response and induce antidepressant-like effect in rats. *Eur Psychiatr*. 2017;41:S366.
81. Herraiz T, Chaparro C. Human monoamine oxidase enzyme inhibition by coffee and beta-carbolines norharman and harman isolated from coffee. *Life Sci*. 2006;78(8):795–802.
82. Moura DJ, Richter MF, Boeira JM, Pêgas Henriques JA, Saffi J. Antioxidant properties of β -carboline alkaloids are related to their antimutagenic and antigenotoxic activities. *Mutagenesis*. 2007;22(4):293–302.
83. Sammi SR, Agim ZS, Cannon JR. From the cover: harmane-induced selective dopaminergic neurotoxicity in *Caenorhabditis elegans*. *Toxicol Sci*. 2018;161(2):335–348.
84. Khan H, Patel S, Kamal M. Pharmacological and toxicological profile of harmane- β -carboline alkaloid: friend or foe. *Curr Drug Metabol*. 2017;18(9):853–857.
85. Walzl A, Unger C, Kramer N, et al. The resazurin reduction assay can distinguish cytotoxic from cytostatic compounds in spheroid screening assays. *J Biomol Screen*. 2014;19(7):1047–1059.
86. Fink SL, Cookson BT. Apoptosis, pyroptosis, and necrosis: mechanistic description of dead and dying eukaryotic cells. *Infect Immun*. 2005;73(4):1907–1916.
87. Gülden M, Jess A, Kammann J, Maser E, Seibert H. Cytotoxic potency of H₂O₂ in cell cultures: impact of cell concentration and exposure time. *Free Radic Biol Med*. 2010;49(8):1298–1305.
88. Mischel RE, Kim YS, Sheldon RA, Ferriero DM. Hydrogen peroxide is selectively toxic to immature murine neurons *in vitro*. *Neurosci Lett*. 1997;231(1):17–20.